Transport of ground-state hydrogen atoms in a plasma expansion

Transport of ground-state hydrogen atoms in a plasma expansion

S. Mazouffre, M. G. H. Boogaarts, I. S. J. Bakker, P. Vankan, R. Engeln, and D. C. Schram
(Received 27 November 2000; revised manuscript received 8 March 2001; published 26 June 2001)

The transport of ground-state atomic hydrogen in the expansion of a thermal plasma generated from an Ar-H_2 mixture is studied by means of laser-based diagnostic techniques. The flow of hydrogen atoms is investigated by two-photon excitation laser-induced fluorescence (LIF), whereas Ar atoms are probed by LIF as well as by UV Rayleigh scattering. The transport of Ar atoms can be fully understood in terms of a free jet flow; H atoms on the contrary exhibit an anomalous behavior. In the course of the plasma expansion, hydrogen atoms decouple from the argon fluid by a diffusion process as a direct consequence of recombination of H atoms at the vessel walls. In this contribution it is shown, on the basis of experimental results, how plasma-surface interactions can strongly influence the flow pattern of an atomic radical fluid.

DOI: 10.1103/PhysRevE.64.016411 PACS number(s): 52.25.Fi, 52.35.Tc, 47.40.Ki, 52.70.−m

I. INTRODUCTION

Understanding the transport of atomic radicals in a plasma expansion, i.e., the flow pattern and the interactions with the surrounding gas, is of interest from several aspects. From a fundamental point of view, a plasma expansion is a very general physical phenomenon that covers a broad range of dimensions, ranging from astrophysical objects [1] to small laser spots [2]. In comparison with the expansion of a neutral gas, plasma expansion is a more complex phenomenon. For instance, different kind of particles are present (neutral, ion, electron, photon), current and electric fields can be generated, and the flow is often not isentropic. From a technological perspective, due to their high reactivity, atomic radicals play a major role in plasma chemistry and therefore are of relevance for industrial applications like deposition of thin films [3,4,5] and surface modification [6].

From a practical point of view, it is advantageous to study the physics of expanding plasmas on the intermediate scale as then the system is well suited for diagnostics. In this contribution, we focus on the transport of ground-state hydrogen atoms in the expansion of a thermal plasma generated from an Ar-H_2 mixture by a dc wall-stabilized arc plasma source. Such a plasma jet can serve as an example, and the results obtained may be generalized to other kind of localized plasma expansion, like solar outbursts and laser spots. Atomic hydrogen is of particular interest. Such a light radical plays an important role in the field of nuclear fusion, e.g., Tokamak plasmas [7], as well as in numerous manufacturing techniques employing processing plasmas. Furthermore, H is one of the main components of both stellar and interstellar matter.

In order to clearly understand the dynamics of such a plasma jet, both neutral Ar atoms and H radicals have to be probed in such a way that the plasma flow is not disturbed. The local argon atom density is monitored by means of UV Rayleigh scattering whereas the Ar velocity and temperature are measured by means of laser induced fluorescence (LIF). The detection of ground-state hydrogen atoms is more cumbersome due to the large energy gap between the electronic ground state and the first excited states. Hydrogen atoms are spatially probed by means of two-photon absorption laser induced fluorescence (TALIF). By applying this method for different positions in the expansion, the H distribution in the plasma jet in terms of density, temperature, and velocity has been completely mapped.

In a foregoing paper [8], we have shown that the transport of H radicals, contrary to that of argon neutrals, cannot be entirely described in terms of the well-established free jet flow picture. Hydrogen atoms exhibit a very specific behavior. Whereas the occurence of a stationary shock wave can clearly be identified on both the temperature profile and the velocity profile along the jet centerline, there is no density discontinuity throughout the shock front. This leads to a nonconservation of the H atom forward flux. It was stated that H radicals can escape the core of the plasma jet by a diffusion process induced by the presence of large density gradients between the jet and its periphery. The latters arise from the recombination of H at the vessel walls that leads to the formation of H_2 molecules. In this contribution, we will analyze in detail the atomic radical anomalous shock wave pattern, and we will demonstrate that the hypothesis of outward diffusion controlled by density gradients can fully explain the measurements. It is also a purpose of this paper to add to the literature detailed measurements of the radical flow characteristics in a plasma expansion.

II. PLASMA JET AND EXPERIMENTAL ARRANGEMENT

The cascaded arc [9] is operated at a 40 A dc current, and with a cathode-anode voltage of 100 V. In normal conditions, a gas flow of 3.0 standard liters per minute (slm) Ar and 0.5 slm H_2 is used. The diameter of the arc channel is 3 mm, the stagnation pressure inside the arc is 0.6 atm and the opening angle of the arc nozzle is 45°.

The cascaded arc thermal plasma expands supersonically into a vacuum vessel (length 3 mm, diameter 0.36 m) where the background pressure (p_{back}) can be varied almost independently from the gas flow, from 10 Pa to 1 atm. Because the plasma expands from the orifice of the arc into a region with a finite pressure, a well-defined free jet shock wave structure [10–12] is produced due to the interaction of the supersonic flow with the ambient gas.

In the case of an Ar-H_2 mixture, a fast lowering in the electron density appears soon after the onset of the expansion [13]. At an electron temperature of 1 eV this ionization loss

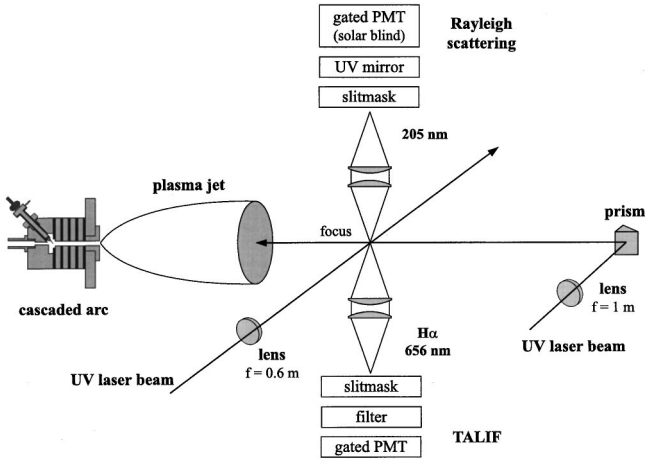

FIG. 1. Schematic view of the experimental arrangement. The plasma is created in a cascaded arc and it expands freely from the source nozzle into a vacuum chamber. The jet diameter is around 50 mm in the subsonic domain (depending on the background pressure), and the vessel diameter is 360 mm. The UV laser beam is used to perform both TALIF and Rayleigh scattering measurements. It can be directed either perpendicular or parallel to the jet axis, which allows for the measurement of $(T_\perp, w_r)$ and $(T_\parallel, w_z)$, respectively.

is due to the production of hydrogen atoms by the associative charge exchange reaction

$$Ar^+ + H_2 \rightarrow ArH^+ + H \quad k = 1.2\times 10^{-15}\ \ m^3\,s^{-1}, \qquad (1)$$

followed by the dissociative recombination reaction [14–16]

$$ArH^+ + e^- \rightarrow Ar + H^* \quad k \approx 10^{-13}\ \ m^3\,s^{-1}. \qquad (2)$$

Thus, using a 6:1 Ar-H_2 mixture, at the arc outlet, the plasma jet turns into almost a gas jet composed of Ar and H atoms and of H_2 molecules. Both the amounts of H and H_2 depend on the dissociation degree of the source that is very likely to be close to 1 [17]. Beyond the Mach disk, the gas expands subsonically and mixes with the residual background gas. Then the evolution of the flow is determined by the circulation pattern in the vessel, which is a direct consequence of the large residence time ($\tau_{res} \approx 1$ s at 20 Pa). Furthermore, as the diffusion time is much shorter than the residence time ($\tau_{diff,H} \approx 1$ ms at 20 Pa), there is ample time for plasma-wall interactions.

In this experiment, ground-state hydrogen atoms are spatially probed by using two-photon absorption laser-induced fluorescence (TALIF) [18–20]. The experimental method is described elsewhere [20,21], and only a short overview is presented here. A simplified scheme of the setup is depicted in Fig. 1. A tunable 20 Hz Nd: yttrium aluminum garnet (YAG) pumped dye laser delivers radiation around 615 nm. The output of the dye laser is frequency tripled using nonlinear optical crystals resulting in 2 mJ of tunable UV light around 205 nm with a measured bandwidth of 0.2 cm^{-1}. The UV laser beam is focused either perpendicular or parallel to the plasma expansion axis.

Hydrogen atoms are excited with two 205 nm photons from the $1s^2S$ ground state to the $3d^2D$ and $3s^2S$ states. The laser beam intensity is low enough to avoid any parasitic effects such as stimulated emission, production of H^+, and dissociation of H_2 molecules. The excitation is monitored by detection of the resulting fluorescence yield on the Balmer-α (H_α) line at 656 nm using a gated photomultiplier tube (PMT). A narrow-band width interference filter ($\Delta\lambda = 10$ nm) is used to isolate the H_α line from the plasma emission. A slitmask is used to define the detection volume (<1 mm^3) which dimensions are smaller than any gradient scale length. The PMT signal is recorded by means of an oscilloscope connected to a computer. The dye laser frequency is calibrated by the simultaneous recording of the absorption spectrum of molecular iodine. From a spectral scan over the two-photon transition, the local H atom density, temperature, and velocity along the laser beam are measured. Note that the measurements are performed in succession. Absolute number densities are obtained by calibrating the TALIF setup by means of a titration reaction with NO_2 in a flow tube reactor [21,22]. To compensate for the pulse-to-pulse energy fluctuation any data point that composes the spectral profile is an average over 256 laser shots.

The UV laser beam at 205 nm is also employed to measure the argon heavy-particle density by means of Rayleigh scattering [23,24]. The polarized, scattered radiation at 205 nm is detected at an angle of 90° using a gated solar blind PMT, as shown in Fig. 1. A dielectric UV mirror centered on 205 nm ($\Delta\lambda = 10$ nm) is used to filter out the plasma background light. The amount of stray light is reduced by means of a set of diaphragms and by using windows at Brewster's angle. Although the amount of photons at 205 nm is much smaller than the amount of photons that can be generated at for instance, 532 nm with our Nd:YAG laser, the differential scattering cross section at 205 nm is about 60 times larger than at 532 nm [25]: $\sigma = 3.6\times 10^{-30}\ m^2$ at 205 nm and $\sigma = 5.6\times 10^{-32}\ m^2$ at 532 nm. The current detection limit in an Ar-H_2 plasma is around $10^{20}\ m^{-3}$: it does not permit us to accurately measure the Ar density in the shock region at a background pressure below 40 Pa.

III. TRANSPORT OF ATOMS ALONG THE JET CENTER LINE

A. Argon atoms

In the case of an expanding argon plasma, it has been demonstrated experimentally [26] that the expansion of neutral atoms can be well understood in terms of an adiabatic supersonic expansion of an ideal gas [10]. Furthermore, the entire axial density profile can be described by a quasi-one-dimensional model based on hydrodynamic equations [26], despite the fact that the Knudsen number *Kn* inside the supersonic domain is rather high. For instance, at a 40 Pa background pressure, $Kn = 0.1$ ahead of the stationary shock wave. Later, this model has been extended to study the case of an expanding argon plasma seeded with a small amount of molecular hydrogen [13].

The development along the jet center line of the Ar heavy particle density, measured by means of UV Rayleigh scatter-

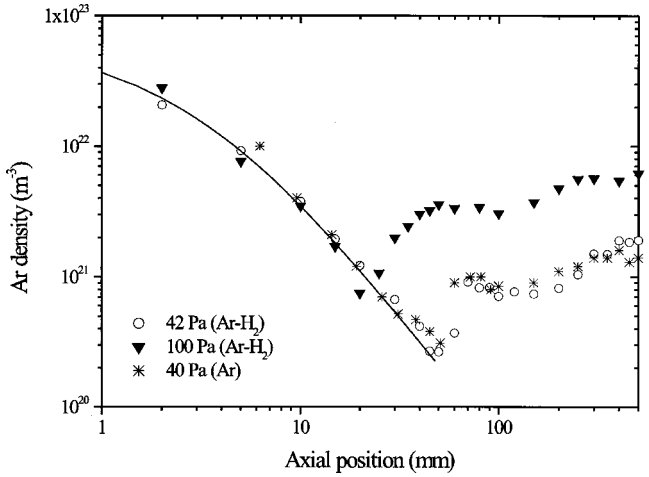

FIG. 2. Axial density profile of Ar neutrals at 42 Pa (open circles) and 100 Pa (solid triangles) background pressure in the case of an Ar-H_2 mixture. The solid line represents a fit using expression (3). Also shown is the Ar axial density profile measured in the case of a pure Ar plasma (star) at $p_{\mathrm{back}}=40$ Pa.

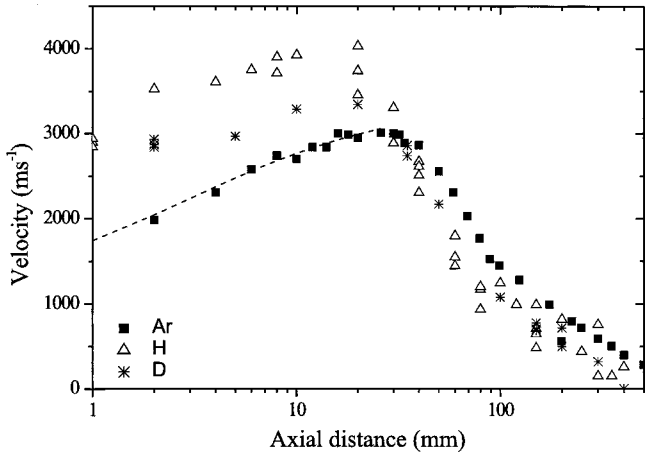

FIG. 3. Axial component of the velocity along the jet centerline for Ar, H, and *D* atoms at a 20 Pa background pressure. The decoupling between H(*D*) and Ar inside the supersonic domain can clearly be seen. The theoretical Ar velocity profile in the supersonic domain (dashed line) is in good agreement with the measurements.

ing for a 6:1 Ar-H_2 mixture, is shown in Fig. 2 for two different background pressures. Our data are in agreement with foregoing measurements obtained in the case of a pure Ar plasma [13], see Fig. 2. It implies that the Ar flow is not disturbed by the presence of H and H_2. From the conservation laws in stationary state, and under the assumption that the particles originate from a point source and flow along straight stream lines, one can obtain the theoretical expression for the density development along the jet centerline

$$n(z)=n_0\frac{z_{\mathrm{ref}}^2}{(z+z_{\mathrm{source}})^2}. \tag{3}$$

In Eq. (3), n_0 is the density in the source, z_{ref} is a scaling length equal to the source nozzle radius in the case of a 45 degrees expansion, and z_{source} is the position of the virtual point source. This formula is similar to the one used to describe the supersonic expansion of an inviscid gas through a sonic orifice in the field of gas dynamics [10,27]. The axial density decay starts at some position z_{source} depending on the source nozzle geometry, e.g., several nozzle diameters in the case of a straight orifice. This decrease in density describes a rarefaction effect due to the increase in the jet cross section.

The measured Ar density profiles in Fig. 2, are fitted according to Eq. (3). As can be seen, the experimental data are well described by the theoretical expression. Up to the stationary shock front the density decrease is not affected by a change in p_{back}, meaning that the supersonic domain of the expansion can be considered as a closed domain surrounded by a shock-wave structure [11,26]. From the fit, both length parameters can be estimated. We find that $z_{\mathrm{ref}}=3.0\pm0.2$ mm and that $z_{\mathrm{source}}=3.0\pm0.2$ mm. This means that the virtual point source, i.e., the start of the expansion, is located 3 mm inside the nozzle. This is a direct consequence of the use of a diverging nozzle. The density jump across the normal shock wave, which results from the conservation of the forward flux, can clearly be seen in Fig. 2. From the Rankine-Hugoniot relation [28] the compression ratio is found to be 3 at 20 Pa and 4, i.e., the maximum compression ratio, at 100 Pa. The slow increase in Ar density in the subsonic region is due to a cooling of the gas by heat transfer, the static pressure being constant. The velocity of Ar atoms in an expanding Ar-H_2 thermal plasma jet created by a cascaded arc, has recently been determined by measuring the Doppler shift in a LIF experiment on metastable Ar [29]. The development of the Ar axial velocity component along the plasma jet axis at $p_{\mathrm{back}}=20$ Pa is shown in Fig. 3.

The general shape of a velocity profile can be described using theory developed in the field of gas dynamics [28], and it has been explained elsewhere for both H atoms [8] and Ar atoms [29]. In short, behind the source exit, the argon gas is first accelerated to supersonic velocities over a few source nozzle diameters due to conversion of thermal energy gained in the source into kinetic energy. If the background pressure is low enough, the flow reaches a steady state, the so-called frozen regime, in which the velocity stays constant. Such a velocity plateau is visible in Fig. 3 for the Ar case. As can also be seen in Fig. 3, in the supersonic domain, the measurements are in good agreement with a theoretical calculation. Then the expanding gas collides with the residual background gas that results in the formation of a stationary shock wave over which the flow experiences a transition from the supersonic to the subsonic regime. Behind the shock, the flow pattern is mainly determined by the geometry of the vessel. The flow velocity decreases due to momentum transfer to the ambient gas particles, and in this regime, the transport of any particles is mainly controlled by diffusion.

B. Hydrogen atoms

1. Anomalous density profile

Contrary to the argon case, hydrogen atom axial density profiles do not exhibit any jump throughout the stationary

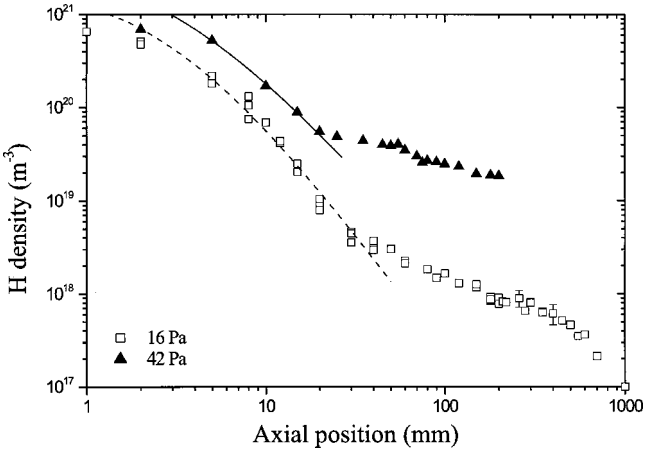

FIG. 4. Axial density profile of H for different background pressures. Contrary to the Ar profiles, there is no density jump throughout the stationary shock front, implying that the forward flux is not conserved. The curves are the result of a fit using Eq. (6).

shock front, as can be seen in Fig. 4, while the drift velocity drops, as can be observed in Fig. 3. This means that the forward flux of H atoms is not conserved in the shock region. This striking demonstration of an anomalous H atom shock pattern has been reported in a foregoing paper [8]. It is postulated that strong density gradients between the core of the jet and its surroundings, due to a low H concentration in the background gas, are responsible for an outward diffusion of H atoms. The efficient destruction of hydrogen ground-state atoms at the wall of the vessel [30], where they recombine to form molecular hydrogen [31–33], is responsible for the very low H background density. In neutral gas mixture expansions migration of the light species towards the edges of the jet has been observed within the first millimeters of the flow [12]. In this region, this so-called mass focusing effect arises from a mass-dependent kinetic energy.

One can exclude under our experimental conditions that H atoms recombine in volume during the expansion process to form molecular hydrogen, which would also lead to a nonconservation of the axial H flux. The chemical reactions that have to be considered are the three-body reactions [34]

$$\begin{aligned} &H+H+Ar\rightarrow H_2+Ar, \quad k=9.8\times10^{-42} \quad m^6\,s^{-1},\\ &H+H+H_2\rightarrow H_2+H_2, \quad k\approx2\times10^{-42} \quad m^6\,s^{-1}, \qquad (4)\\ &H+H+H\rightarrow H_2+H, \quad k=4.5\times10^{-44} \quad m^6\,s^{-1}, \end{aligned}$$

as well as the two-body reaction[35]

$$H+H\rightarrow H_2 \quad k=10^{-21} \quad m^3\,s^{-1}. \qquad (5)$$

Furthermore, as already mentioned in Ref. [8], the steepness of the density decay within the supersonic domain depends on p_{back}, which means that H atoms that come from the source receive information about the standing ambient gas. This proofs that a shock-wave structure does not form a totally closed system. As shown in Fig. 4, the H axial density profile ahead of the shock wave can be well described by a modified point source expansion law of the form

$$n(z)=n_0\frac{z_{\mathrm{ref}}^{\beta}}{(z+z_{\mathrm{source}})^{\beta}}. \qquad (6)$$

where the exponent β is larger than two, because an outward diffusion effect is superimposed on the normal rarefaction effect. The length parameters z_{ref} and z_{source} are taken to be the ones determined from the Ar measurements. The values of n_0 and β depend on p_{back} and are listed in Table I. It can clearly be seen that β gets closer to two as the pressure increases, meaning that H atoms get better confined inside the supersonic jet. In other words, it becomes more difficult for H to cross the barrel shock wave at high p_{back}, since the local mean free path decreases. This also explains why the H density behavior in the ambient gas depends on p_{back}, as can be seen in Fig. 4.

2. Perpendicular temperature

The axial profile of the atomic hydrogen perpendicular temperature $T_{\perp}$ (associated with the velocity distribution perpendicular to a stream line) is depicted in Fig. 5 for two different values of p_{back}. The temperature profiles clearly reveal the presence of a stationary shock front across which $T_{\perp}$ raises due to the conversion of the jet particle kinetic energy into random thermal motion. As predicted by the theory, both the position and the width of the shock front depend on p_{back} [12]. In the supersonic region of the expansion, a strong cooling effect occurs because the thermal energy gained by the particles in the plasma source is converted into kinetic energy by means of collisions. For an adiabatic process, the energy equation can be replaced by the Poisson adiabatic law [28]

$$\left(\frac{n}{n_0}\right)^{\gamma-1}=\frac{T}{T_0}, \qquad (7)$$

TABLE I. Parameters governing the H atom expansion at different background pressures. The subscript *o* refers to the source region. The variable β is linked to the on-axis H atom density decay, see Eq. 6, and γ is the quasiadiabatic exponent.

p_{back} (Pa)	16	20	42	100
$n_o(m^{-3})$	$(5.6\pm1.0)\times10^{21}$	$(2.2\pm0.2)\times10^{21}$	$(5.6\pm1.0)\times10^{21}$	$(2.2\pm0.2)\times10^{21}$
β	2.65 ± 0.10	2.35 ± 0.05	2.20 ± 0.05	2.10 ± 0.05
γ	1.40 ± 0.10	1.40 ± 0.04	1.50 ± 0.15	1.45 ± 0.05
T_o (K)	9000 ± 3000	4800 ± 600	8100 ± 3500	5600 ± 800

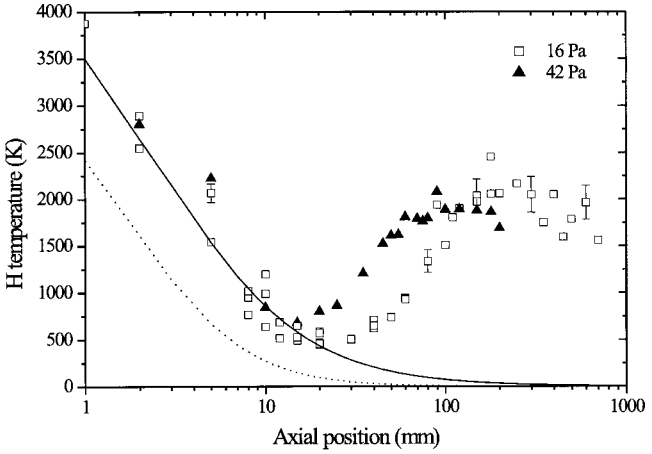

FIG. 5. H perpendicular temperature profile along the jet centerline for two different background pressures. Also shown are the theoretical temperature profiles with $\gamma=1.45$ (solid line) and with $\gamma=5/3$ (dashed line). The source temperature is found to be 0.5 eV.

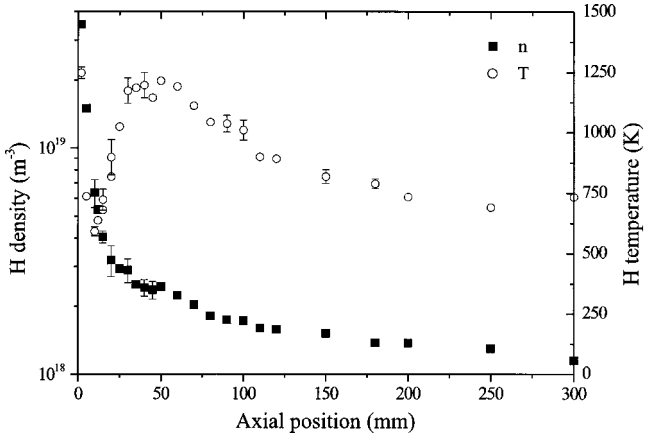

FIG. 6. Axial profiles of the H density and H perpendicular temperature $T_\perp$ when He is used as a carrier gas instead of Ar. The shock front structure is visible in the temperature profile. However, no discontinuity is observed in the H density profile.

where γ is the adiabatic exponent which is equal to 5/3 for a monoatomic gas. By plotting the H atom temperature as a function of the density, the isentropic exponent can be evaluated. The value of γ for various values of p_{back} is listed in Table I. As can be seen, γ for H radicals has the almost constant value 1.4. The fact that the measured γ is smaller than the theoretical γ for a monoatomic gas means that, contrary to a neutral gas expansion, the supersonic expansion of a plasma is nonadiabatic [36]. As can be seen in Fig. 5, the measured temperature is well above the theoretical isentropic temperature. In the case of a plasma expansion, the cooling of neutrals in the supersonic domain can be disturbed by heat transfer from both the source and the hot background gas behind the shock front. Re-entry of background gas into the supersonic domain through the barrel shock wave can also disturb the flow, especially at low pressure [29]. In Fig. 5, a fit to the measured data is shown using the adiabatic law with measured β and γ. The source temperature T_0, that corresponds to the temperature inside the arc nozzle, is found to be close to 0.5 eV, independent of p_{back}.

3. Axial velocity component

The measured axial profiles of the axial velocity components of H and *D* are shown in Fig. 3 for a background pressure of 20 Pa. Also the Ar velocity profile is shown. The shape of the H and *D* velocity profile along the jet center line is very similar to the Ar one. This means that the mechanisms responsible for the H and *D* axial velocity development are connected to those that determine the Ar profile. Throughout the supersonic domain, the H(*D*) velocity is higher than the Ar velocity. The decoupling between the Ar fluid and the radical fluid, which is already present at the source exit, is a direct consequence of losses of H atoms at the walls. A possible way of describing the hydrogen drift velocity is to consider this velocity as the sum of the argon drift velocity and a diffusion term. The diffusion velocity, that contains implicitly the H-density gradients, would control the H flow relative to the Ar flow. More theoretical and computational works are needed to validate this idea. Nonetheless, primary works using an hydrodynamic approach to model the Ar-H flow, seem to confirm this view. Behind the shock wave, all velocities are about the same, meaning that all particles are well coupled. This is a consequence of the much higher collision frequency in the subsonic domain. However, across the stationary shock front, the velocities differ substantially, the atomic hydrogen velocity being lower than the argon velocity. Because of collisions in the shock, we can expect the difference in velocity to slowly diminish. It can also be seen that the H(*D*) velocity starts to decrease earlier than the Ar velocity. This effect is not yet well understood.

IV. USE OF A LIGHT CARRIER GAS

In order to study the influence of the mass on the radical transport mechanism, the carrier gas has been changed: argon ($m_{\text{Ar}}=40$ amu) has been replaced by helium ($m_{\text{He}}=4$ amu). The parameters are the following: the arc current is 50 A, the cathode-anode voltage is 140 V, the He flow is 2 slm, the H_2 flow is 0.5 slm and the background pressure is 20 Pa. The source geometry is identical to the one used in the Ar-H_2 mixture case. An admixture of less than 2% Ar gas is used to prevent a too fast degradation of the cascaded arc cathode tips. Thus, the average mass of the mixture is equal to 4.3 amu, using the fact that the plasma source delivers mainly H_2 in view of the low measured H density, see Fig. 6.

The results of the measurements are given in Fig. 6. The H density at the source exit is much less, by nearly 2 orders of magnitude at $p_{\text{back}}=20$ Pa, than when Ar is used as a carrier gas [8]. The relatively low-delivered amount of H arises directly from the way H atoms are created in a He-H_2 mixture [37–39]. The low H temperature at the arc outlet is due to the high-thermal conductivity of the He-H_2 mixture.

The sharp rise in the temperature, which occurs behind the arc exit as depicted in Fig. 6, reveals the occurrence of a stationary shock front. In comparison with the results obtained at the same p_{back} for an Ar-H_2 mixture, two remarks

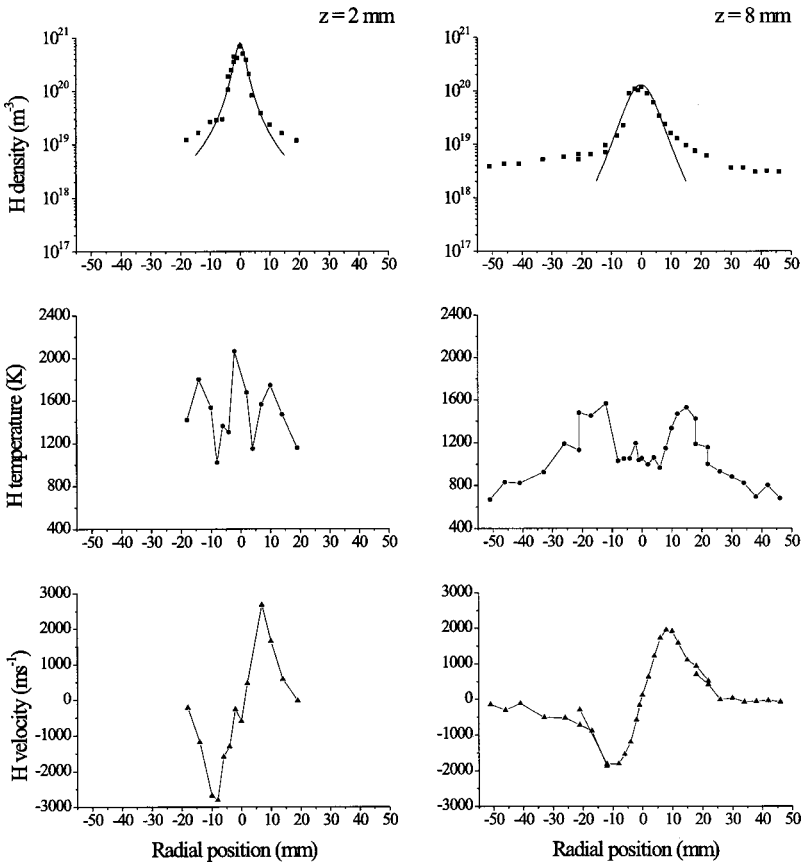

FIG. 7. Radial profiles of the density (top), perpendicular temperature $T_\perp$ (middle), and radial velocity w_r (bottom) of H atoms for a background pressure of 16 Pa at $z=2$ mm (left) and $z=8$ mm (right). The H density profile in the core of the jet is modeled using Eq. (8) (solid line) with $a=2.4$ and 5.5 at $z=2$ and 8 mm, respectively.

can be made. First, the shock wave is located very close to the arc exit since the shock position varies with the stagnation pressure, which at constant flow decreases when the atomic mass decreases [12]. Second, the shock front, whose thickness is always in the order of one local mean free path for momentum exchange, is narrow despite a relatively low neutral-neutral momentum exchange cross section for He. This originates from the fact that the shock wave occurs close to the nozzle exit, where the He density is still high.

According to the temperature jump, the Mach number M is found to be equal to 2.3 ahead of the shock when using the Rankine-Hugoniot relation with a value of 1.5 for the isentropic exponent γ. With this value for M, the amplitude of the density jump should be 2.8. However, no significant density jump is observed across the shock wave. This again indicates an outward diffusion of H atoms. Despite the small mass ratio between He and H, H atoms leave the core of the plasma jet and recombine at the vessel wall. This result points out the importance of the density gradients in the H atom loss process.

In the subsonic domain of the flow, the temperature decays fast because of the large thermal conductivity of the mixture, and the density remains relatively constant. Despite the low H density at the source outlet, it is slightly higher behind the stationary shock wave ($z>100$ mm) than in the case where Ar is used as a carrier gas. This means that H is better transported when the mass of the carrier gas is small. The gain in confinement when the mass of the carrier gas is closer to that of the transported species is known for mylticomponent neutral beam expansions [12]. But we demonstrated that despite a better confinement, the atomic hydrogen anomalous shock-wave pattern does not vanish. A better transport is of relevance for the downstream chemistry since the amount of ground-state radicals can be one of the limiting factors when an expanding plasma jet is used for thin film deposition [5] or surface modification. Then a good compromise has to be found between the quantity of radicals available in front of the surface and the momentum of the carrier gas, which is also used to transport other particles like molecules of the precursor gas.

V. CONFINEMENT OF RADICALS INSIDE THE JET CORE

In order to have a better insight in the lack of confinement of atomic hydrogen inside the core of the plasma jet generated from an Ar-H_2 mixture, it is of interest to study beam cross sections at several axial positions. Also the permeability of the Ar barrel shock wave needs to be discussed. In Figs. 7, 8, and 9, radial profiles of the H atom density, perpendicular temperature, and radial velocity component are given for $p_{\mathrm{back}}=16$ Pa at $z=2$, 8, 20, 50, 80, and 100 mm behind the arc outlet.

A. Radial profiles of the H density

From the radial density profiles, we observe that the density of atomic hydrogen decreases fast as we move away from the source exit. This is a direct consequence of the rarefaction effect due to the increase of the beam diameter.

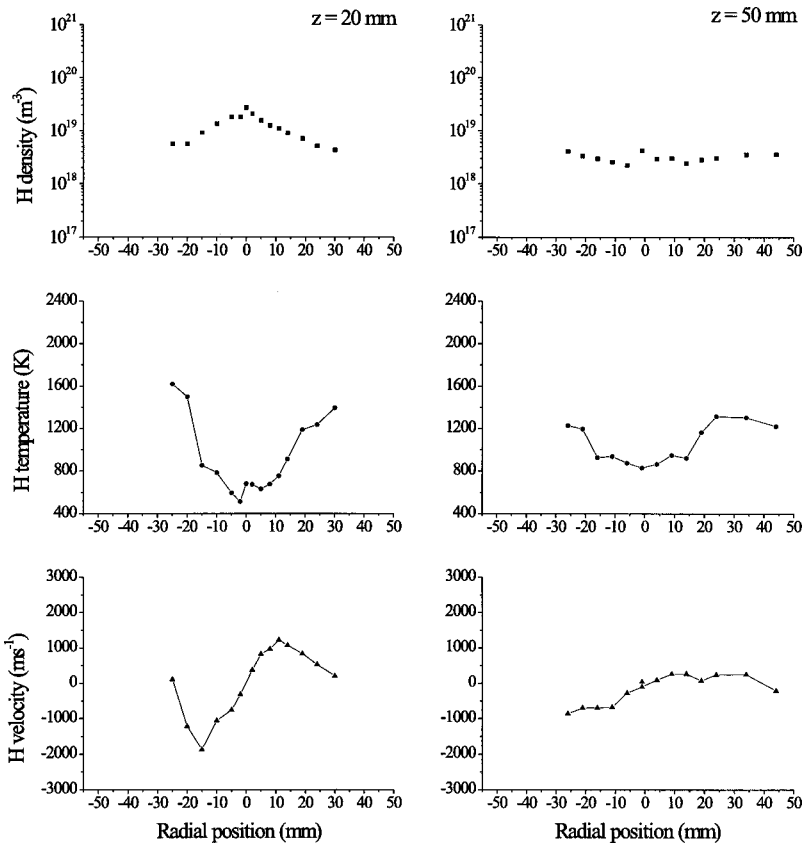

FIG. 8. Radial profiles of the density (top), perpendicular temperature $T_\perp$ (middle), and radial velocity w_r (bottom) of H atoms for a background pressure of 16 Pa at $z=20$ mm (left) and $z=50$ mm (right).

However, this effect is enlarged by the outward diffusion phenomenon. Contrary to argon, the H jet is never overexpanded, i.e., the H atom density inside the jet is never lower than outside the jet. Across the stationary shock front, from $z=50$ to 100 mm, the radial H density profile is flat because the diffusion process levels out the density profile.

The shape of the density profile in the core of the plasma beam can be theoretically described. Such a shape corresponds to a situation in which the jet is underexpanded. We propose the following function

$$n(r,z)=n(z)\cos^a(\varphi), \tag{8}$$

with the angle φ given by

$$\varphi=\arctan\left(\frac{r}{z+z_{\text{source}}}\right), \tag{9}$$

where r is the radial distance and z_{source} is the position of the virtual point source. In the field of gas dynamics, some more complex functions have been proposed based on experimental data [10,40]. The results of fits using Eq. (8) are depicted in Fig. 7 at $z=2$ and 8 mm. As can be seen in the graph, the function reasonably represents the experimental data inside the jet. However, to obtain such an agreement, the exponent a in Eq. (8) has to be modified when changing the axial position z: $a=2.4$ at $z=2$ mm and $a=5.5$ at $z=8$ mm. In the classic supersonic expansion picture, the value of this exponent only depends on the source conditions and geometry and on γ, but it is a constant in the course of the expansion. Once more the increase in a is connected to an outward loss of H radicals in particular in the outward regions of the jet.

B. Temperature and radial velocity

The radial profiles of the H atom perpendicular temperature $T_\perp$ clearly show evidence of the quasiadiabatic cooling effect. They also reveal the structure of the barrel shock wave.

It can be seen in Fig. 7 that at $z=2$ mm in the core of the jet $T_\perp$ is not constant. The temperature is higher on axis than on the sides. This is purely a geometrical effect: the H atoms detected on the sides have travelled more in comparison with those on the jet axis. Then, since the former have undergone more collisions they converted a larger part of their thermal energy into kenetic energy that leads to a lower temperature. At $z=8$ mm, this geometrical effect is almost not noticeable anymore.

The rise in $T_\perp$ when going off axis is due to collisions with Ar atoms in the barrel shock wave [12]. This temperature jump defines the boundary of the plasma jet. Then, behind the barrel shock wave, $T_\perp$ decreases towards the vessel walls because of heat transfer to the background gas. As can be seen in Fig. 7, the background gas temperature is rather low, around 500 K. In the subsonic domain, the temperature of flowing H atoms is homogeneous over the jet radius, as can be seen in Fig. 9, and relatively high. This shows that the heat gained in the source is transported mainly forward with some radial losses due to thermal conduction.

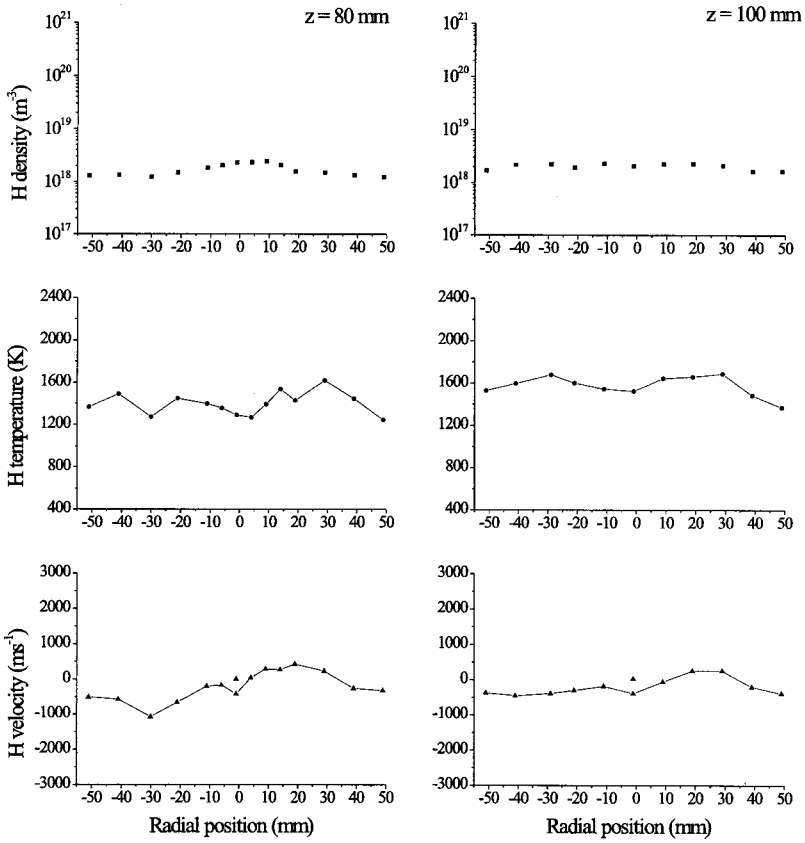

FIG. 9. Radial profiles of the density (top), perpendicular temperature $T_\perp$ (middle), and radial velocity w_r (bottom) of H atoms for a background pressure of 16 Pa at $z=80$ mm (left) and $z=100$ mm (right).

The radial profiles of the H atom radial velocity component also reveal the Ar shock-wave structure. Because of the expansion process, the radial velocity first increases when moving away from the jet axis. Then when H atoms collide with Ar atoms in the barrel shock wave, the velocity decreases since it is converted into thermal energy, and the temperature increases accordingly. As expected, the position of the Ar barrel shock as deduced from the H radial velocity profile does coincide with the position deduced from the corresponding $T_\perp$ profile.

As can be seen in Figs. 7 and 8, the maximum value of the H radial velocity $w_r^{\max}$ decreases as z increases. This is not predicted in the classical expansion picture. Assuming that the total velocity does not vary with the radial position, the magnitude of the radial velocity component as a function of the radial position for a given axial position can be written in the classical picture as follows

$$w_r = w_{z,0}\sin(\varphi), \tag{10}$$

where $w_{z,0}$ is the axial speed at $r=0$ and φ is the expansion angle given by Eq. (9). In the case of a free jet, the maximum radial velocity is always reached at roughly the same angle φ for a given p_{back} independent of z. Since up to the stationary shock wave the axial velocity increases slightly, as can be seen in Fig. 3, $w_r^{\max}$ should then also increase a bit. However, it decreases by approximately a factor 3 between $z=2$ and 20 mm. By using the measured argon axial drift velocity, shown in Fig. 3, it is possible to estimate with Eq. (10) the maximum value of the H radial velocity component in case of a perfect coupling between H radicals and Ar atoms. The velocity is calculated at the boundary of the plasma jet of which the location is taken from the $T_\perp$ profile. The maximum speed is found to be equal to 1000, 900, and 900 ms^{-1} at $z=2$, 8, and 20 mm, respectively. At any z, the highest H radial velocity is always larger than the calculated value, which points out the importance of the radial escape of H radicals. This radial escape process is certainly most important at the beginning of the plasma expansion where the atomic hydrogen radial velocity component is highest.

The discrepancy between the expected H radial velocity and the measured one not only confirms the idea of a decoupling between H and Ar atoms, but it also suggests that the H velocity is connected to the H density gradients, which are the largest at the beginning of the expansion and that decrease with increasing z.

C. Permeable Ar barrel shock wave

The picture of a strong decoupling between H and Ar is substantiated by comparing the radial profile of the axial and radial velocity of the H atoms and the radial velocity components of the Ar atoms [29]. This is done in Fig. 10 for a position of 8 mm behind the arc outlet and at $p_{\text{back}}=20$ Pa. The data points are plotted as a function of the angle φ with the expansion axis given by Eq. (9).

This figure confirms the picture of an outward diffusion of H. Moreover, it can be fully understood by considering that the H density gradient is the driving mechanism of the diffusion process. First, the graph clearly shows the decoupling

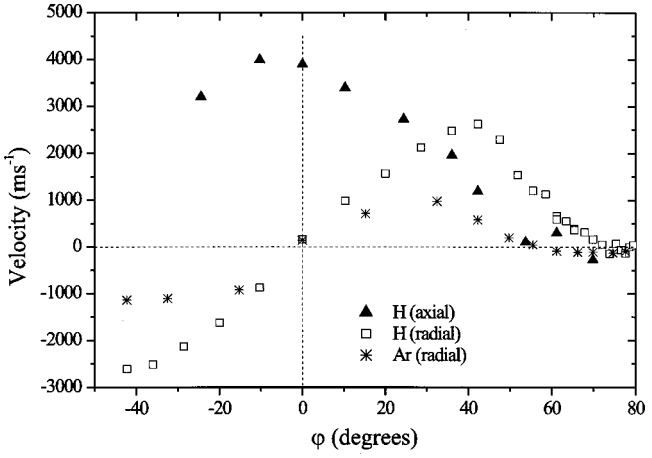

FIG. 10. Profiles of the axial and radial component of the H velocity as well as the radial component of the Ar velocity as a function of the angle with the jet axis, recorded at $z=8$ mm behind the arc nozzle.

between H and Ar atoms. On the expansion axis, both radial velocity components are zero. As r increases, i.e., further from the axis, the gap between the two velocities also increases, the maximum H radial speed being approximately three times higher than the maximum Ar speed. Second, H atoms penetrate and even cross the Ar barrel shock. The decay in Ar radial velocity, due to friction with the standing gas, indicates the position of the barrel shock. It follows from the picture that at $z=8$ mm, the expansion angle is about 30°. But the H atom radial velocity only starts to decrease beyond the beginning of the Ar barrel shock wave. Moreover, when the Ar velocity is zero, the H velocity is still high, indicating that H atoms are still moving radially into the background gas, where Ar atoms are motionless. Finally, the H velocity becomes zero because of increasing friction with the neutral background gas. Then the directed motion is replaced by a random motion due to the thermal speed. Third, even if H atoms penetrate the Ar barrel shock wave with still a significant axial velocity component, H mainly escapes the plasma jet radially. Indeed, the axial velocity component becomes zero whereas the radial component is still high. This is a direct consequence of the steep radial density gradients between the core of the plasma beam and its vicinity.

VI. ATOMIC HYDROGEN DIFFUSION FLUX

To confirm the fact that hydrogen atoms escape the core of the plasma jet by a diffusion process we estimate, at a background pressure of 16 Pa, the losses of H radicals over the normal shock wave, i.e., from $z=20$ mm to $z=100$ mm, and compare them with a calculated diffusion flux.

The loss of atomic radicals in the shock region can be estimated by determining the difference between the forward flux of H atoms entering the shock front, ϕ_H^{in}, and the flux behind the shock, ϕ_H^{out}. At a given z, the forward flux (in s^{-1}) is given by

$$\phi^{\text{forward}}=\int\int_S nwdS=\int_0^R n_x(r)w_z(r)2\pi r dr, \quad (11)$$

where R represents the position of the boundary of the jet that is taken to be the radial position at which the H atom radial velocity is maximum. In order to calculate the forward flux, the radial profile of the H axial velocity component is needed. We will assume that the profile is identical to the one measured at $z=8$ mm, which, in the core of the jet, can be well approximated by

$$w_z(r)=w_z(0)\cos^2(\varphi), \quad (12)$$

where the expansion angle φ is given by Eq. (9). We find that $\phi_H^{\text{in}}=3.3\times10^{19}\,s^{-1}$ and $\phi_H^{\text{out}}=3.9\times10^{18}\,s^{-1}$, which means one order of magnitude loss of H flux.

Now this loss of H radicals has to be compared with the H radial flux across the shock front. At a specific axial position z, the differential radial flux of H atoms at the jet boundary R is given by

$$\frac{\partial}{\partial z}\phi_H^{\text{rad}}=2\pi R n(z,R)w_r(z,R). \quad (13)$$

With our data set, only an averaged H atom radial flux $\overline{\phi_H^{\text{rad}}}$ can be calculated over the shock front. The latter is obtained by multiplying the averaged differential flux by the shock thickness L, which is equal to 80 mm at 16 Pa. We find that $\overline{\phi_H^{\text{rad}}}=3.4\times10^{19}\,s^{-1}$, which is in good agreement with the decrease in forward flux. Thus, we find that the total H atom flux is conserved throughout the shock front.

Finally, the radial flux can be compared with a diffusion flux. An estimate of the thermal flux can be obtained by using Fick's diffusion law. The radial diffusion flux of H atoms through the stationary shock wave is given by

$$\phi_H^{\text{th}}=-\lambda^{H\text{-Ar}}v_{\text{th}}\frac{\partial n_H}{\partial r}S=\frac{v_{\text{th}}}{n_{\text{Ar}}\sigma_{\text{Ar-H}}}\frac{\partial n_H}{\partial r}S, \quad (14)$$

where $\sigma_{\text{Ar-H}}$ is the momentum transfer cross section [41], v_{th} is the H atom thermal speed, and $S=2\pi RL$ is the surface around the stationary shock wave. The H atom density gradient between the jet and the vessel wall can be estimated from

$$\frac{\partial n_H}{\partial r}=\frac{n_H(R)-n_H(wall)}{R-r_{\text{vessel}}}\approx\frac{n_H(R)}{R-r_{\text{vessel}}}, \quad (15)$$

where $r_{\text{vessel}}=180$ mm is the radius of the vacuum chamber. From Rayleigh scattering measurements [13,26], the average Ar density at the jet boundary is found to be equal to $6\times10^{20}\,m^{-3}$. The H diffusion flux is then equal to $3.2\times10^{19}\,s^{-1}$. This value is in good agreement with those calculated previously. It thus confirms the picture of radial outflow induced by a density gradient.

VII. CONCLUSIONS

In the expansion of a plasma generated from an Ar-H_2 mixture, hydrogen atoms are decoupled from argon atoms. As a consequence, a peculiar situation is created where the plasma flow is composed of two fluids with their own macroscopic features. The Ar flow pattern can be entirely described using the well-established inert gas supersonic expansion theory. On the contrary, the H flow pattern exhibits a significant departure from the classical expansion theory. The anomalous H atom flow characteristic is a direct consequence of the interaction between the plasma and the vessel walls where H atoms recombine to form molecular hydrogen.

The decoupling effect, of which the strength depends on the background pressure and on the reduced mass, is a general physical phenomenon that applies to most of atomic radicals as soon as the plasma expansion is surrounded by surfaces where the radicals can recombine with a high probability. In that case the surfaces, e.g., a reactor wall or dust particles, act as a sink for the radical. This in turn creates density gradients that are the driving force for this effect.

ACKNOWLEDGMENTS

The authors would like to acknowledge fruitful discussion with Professor M. C. M. van de Sanden and Dr. J. A. M. van der Mullen. The authors greatly appreciate the skillful technical assistance of M. J. F. van de Sande, A. B. M. Hüsken, and H. M. M. de Jong. This work is part of the research program of the Netherlands Foundation for Fundamental Research on Matter (FOM) and is partially founded by Euratom. It is also financially supported by the Netherlands Organization for Scientific Research (NWO).

[1] *Beams and Jets in Astrophysics*, edited by P. A. Hugues (Cambridge University, Cambridge, 1991).
[2] A. Lebéhot and R. Campargue, Phys. Plasmas **3**, 2502 (1996).
[3] M. Veiler, S. Sattel, T. Giessen, K. Jung, H. Ehrhardt, V. S. Veerasamy, and J. Robertson, Phys. Rev. B **53**, 1594 (1996).
[4] M. C. M. van de Sanden, R. J. Severens, W. M. M. Kessels, R. F. G. Meulenbroeks, and D. C. Schram, J. Appl. Phys. **84**, 2426 (1998).
[5] W. M. M. Kessels, J. P. M. Hoefnagels, M. G. H. Boogaarts, D. C. Schram, and M. C. M. van de Sanden, J. Appl. Phys. **89**, 2065 (2001).
[6] S. Veprřek, J. Patscheider, and J. Th. Elmer, Plasma Chem. Plasma Process. **8**, 445 (1988).
[7] J. Wesson, *Tokamak* (Clarendon, Oxford, 1997).
[8] S. Mazouffre, M. G. H. Boogaarts, J. A. M. van der Mullen, and D. C. Schram, Phys. Rev. Lett. **84**, 2622 (2000).
[9] G. M. W. Kroesen, D. C. Schram, and J. C. M. de Haas, Plasma Chem. Plasma Process. **10**, 551 (1990).
[10] H. Ashkenas and F. S. Sherman, in *Proceedings of Rarefied Gas Dynamics* (Academic, New York, 1966), Vol. 4, p. 84.
[11] E. P. Muntz, B. B. Hamel, and B. L. Maguire, AIAA J. **8**, 1651 (1970).
[12] *Atomic and Molecular Beam Methods*, edited by G. Scoles (Oxford University, New York, 1988).
[13] R. F. G. Meulenbroeks, R. A. H. Engeln, M. N. A. Beurskens, R. M. J. Paffen, M. C. M. van de Sanden, J. A. M. van der Mullen, and D. C. Schram, Plasma Sources Sci. Technol. **4**, 74 (1995).
[14] R. F. G. Meulenbroeks, A. J. van Beek, A. J. G. van Helvoort, M. C. M. van de Sanden, and D. C. Schram, Phys. Rev. E **49**, 4397 (1994).
[15] P. Gaucherel and B. Rowe, Int. J. Mass Spectrom. Ion Phys. **25**, 211 (1977).
[16] P. Tosi, O. Dmitrijev, Y. Soldo, D. Bassi, D. Cappelletti, F. Pirani, and V. Aquilanti, J. Chem. Phys. **99**, 985 (1993).
[17] R. F. G. Meulenbroeks, R. A. H. Engeln, J. A. M. van der Mullen, and D. C. Schram, Phys. Rev. E **53**, 5207 (1996).
[18] J. Bokor, R. R. Freeman, and R. H. Storz, Phys. Rev. A **24**, 612 (1981).
[19] U. Czarnetzki, K. Miyazaki, T. Kajiwara, K. Muraoka, M. Maeda, and H. F. Döbele, J. Opt. Soc. Am. B **11**, 2155 (1994).
[20] H. W. P. van der Heijden, M. G. H. Boogaarts, S. Mazouffre, J. A. M. van der Mullen, and D. C. Schram, Phys. Rev. E **61**, 4402 (2000).
[21] S. Mazouffre, M. G. H. Boogaarts, R. Engeln, J. A. M. van der Mullen, and D. C. Schram, *Proceedings of Laser-Aided Plasma Diagnostics* (Lake Tahoe, California, 1999), p. 320.
[22] A. D. Tserepi, J. R. Dunlop, B. L. Preppernau, and T. A. Miller, J. Vac. Sci. Technol. A **10**, 1188 (1992).
[23] T. V. George, L. Goldstein, L. Slama, and M. Yokoyama, Phys. Rev. **137**, 369 (1965).
[24] S. C. Snyder, L. D. Reynolds, G. D. Lassahn, J. R. Fincke, C. B. Shaw, Jr., and R. J. Kearney, Phys. Rev. E **47**, 1996 (1993).
[25] G. I. Chashchina, V. I. Gladushchak, and E. Ya. Shreider, Opt. Spectrosc. **24**, 1008 (1968).
[26] M. C. M. van de Sanden, J. M. de Regt, and D. C. Schram, Plasma Sources Sci. Technol. **3**, 501 (1994).
[27] H. C. W. Beijerinck, R. J. F. van Gerwen, E. R. T. Kerstel, J. F. M. Martens, E. J. W. van Vliembergen, M. R. Th. Smits, and G. H. Kaashoek, Chem. Phys. **96**, 153 (1985).
[28] L. Landau and E. Liftshitz, *Fluid Mechanics* (Pergamon, London, 1989).
[29] R. Engeln, S. Mazouffre, P. Vankan, D. C. Schram, and N. Sadeghi (unpublished).
[30] P. Kae-Nune, J. Perrin, J. Jolly, and J. Guillon, Surf. Sci. Lett. **360**, L495 (1996).
[31] R. I. Hall, I. Cadez, M. Landau, F. Pichou, and C. Shermann, Phys. Rev. Lett. **60**, 337 (1995).
[32] P. J. Eenshuistra, J. H. M. Bonnie, J. Los, and H. J. Hopman, Phys. Rev. Lett. **60**, 341 (1988).
[33] M. Persson and B. Jackson, J. Chem. Phys. **102**, 8 (1998).
[34] N. Cohen and K. R. Westberg, J. Phys. Chem. Ref. Data **2**, 531 (1983).
[35] L. E. Kline, W. D. Partlow, and W. E. Bies, J. Appl. Phys. **65**, 70 (1989).

[36] R. B. Fraser, F. Robben, and L. Talbot, Phys. Fluids **14**, 2317 (1971).
[37] E. Grant Jones, R. L. C. Wu, B. Mason Hughes, T. O. Tiernan, and D. G. Hopper, J. Chem. Phys. **73**, 5631 (1980).
[38] R. Johnsen, A. Chen, and M. A. Biondi, J. Chem. Phys. **72**, 3085 (1980).
[39] H. Tawara, J. Phys. Chem. Ref. Data **19**, 617 (1990).
[40] A. H. M. Habets, Ph.D. thesis, Eindhoven University of Technology, The Netherlands, 1977 (unpublished).
[41] A. V. Phelps, J. Phys. Chem. Ref. Data **21**, 883 (1992).